AIAA JOURNAL
Vol. 31, No. 9, September 1993

Effect of Curvature on Stationary Crossflow Instability of a Three-Dimensional Boundary Layer

Ray-Sing Lin* and Helen L. Reed†
Arizona State University, Tempe, Arizona 85287

An incompressible three-dimensional laminar boundary-layer flow over a swept wing is used as a model to study both the wall-curvature and streamline-curvature effects on the stationary crossflow instability. The basic state is obtained by solving the full Navier-Stokes (N-S) equations numerically. The linear disturbance equations are cast on a fixed, body-intrinsic, curvilinear coordinate system. Those nonparallel terms which contribute mainly to the streamline-curvature effect are retained in the formulation of the disturbance equations and approximated by their local finite difference values. The resulting eigenvalue problem is solved by a Chebyshev collocation method. The present results indicate that the convex wall curvature has a stabilizing effect, whereas the streamline curvature has a destabilizing effect. A validation of these effects with an N-S solution for the linear disturbance flow is provided.

I. Introduction

THREE-DIMENSIONAL boundary-layer stability and transition on a swept wing has become an increasingly important research subject for the effective application of laminar flow control. A recent review is given by Reed and Saric.[1] Although there are a variety of instability mechanisms that may cause transition in a swept-wing boundary layer, the present work focuses on the study of the stationary crossflow instability. According to Bippes,[2] Kohama et al.,[3] and Radeztsky et al.,[4] flows with low turbulence levels reveal dominating stationary vortices, and these provide the mechanism for breakdown; traveling modes appear to play a passive role.

The state of the art in swept-wing design still involves the use of linear stability theory. Stuart (Gregory et al.[5]) was the first to derive the three-dimensional linear stability equations for application to the rotating-disk flow. He also determined a transformation reducing the three-dimensional temporal problem to a two-dimensional one. Independently, Kobayashi et al.[6] and Malik et al.[7] showed that the Coriolis force and streamline curvature have a very stabilizing effect on disturbances in a rotating-disk flow. Although both groups reported almost identical critical Reynolds numbers, their formulations of the streamline-curvature effect were different. These differences have been commented on by Mack[8] and Spalart.[9] Spalart conducted direct Navier Stokes (N-S) simulations and confirmed that correct theories should include the curvature terms.

For nonrotating three-dimensional boundary-layer flow, Malik and Poll[10] adopted Stuart's theory and studied the incompressible flow over the windward face of a yawed infinite cylinder and reported that the location of transition had an N factor of 11, as compared with 17 when the effects of curvature were neglected. However, this work contained the surface curvature and was inconclusive as far as the streamline-curvature effects were concerned. To apply Stuart's stability theory, one must guess the wave direction, which is part of the solution and is generally difficult to approximate. Malik and Poll suggested iteratively rotating the coordinate system until one of the coordinate axes aligns with the wave number vector. Then the local growth rates are obtained. Two metric terms m_{12} and m_{21} associated with the final coordinate system are claimed (in that paper) to provide the effects of streamline curvature. (For definitions of m_{12} and m_{21} see Ref. 5.) This seems to be difficult to justify for three reasons.

First, there is no unique coordinate system satisfying tangency to the wave number vector, and hence the values of m_{12} and m_{21} can depend on the choice of the trial coordinate system. Second, to overcome the pressure force in the crossflow direction, near the wall in a swept-wing boundary layer, the flow must follow streamlines that are more curved than the local inviscid streamlines. Thus, streamline curvature must vary with the normal direction, and typically m_{12} and m_{21} are locally taken as constants. Third, streamline curvature is actually induced by the spatial variations of the basic state, which have long been known as "nonparallel effects." In previous work, these have been routinely neglected.

In this work, a finite difference method to account for streamline curvature in the disturbance equations is presented. The basic state is a three-dimensional incompressible boundary-layer flow obtained from a full N-S simulation. The linear stability of this flow is then examined and the individual effects of streamline curvature and wall curvature are determined for the stationary crossflow instability. A validation of these effects with a linear N-S solution for the disturbance flow is provided.

II. Streamline-Curvature and Wall-Curvature Effect

Figure 1 shows schematically the geometry and the main notation of the fixed body-intrinsic coordinate system used. The conical-flow assumption is used for the basic state, which implies invariance of the pressure and velocities in the spanwise direction z, and the x- and y-momentum equations decouple from the z-momentum equation. Details of the geometric parameters and the results of the basic-state calculations are provided in Sec. V.A.

The evolution of infinitesimally small disturbances superimposed on a basic state is considered, so that the instantaneous nondimensional velocities u,v, and w and pressure p can be expressed as

$$q(x, y, z, t) = \bar{Q}(x, y) + q'(x, y, z, t) \tag{1}$$

where $q = (u, v, w, p)$, and barred and primed quantities represent basic-state and disturbance-state quantities, respectively. To nondimensionalize the governing equations, the infinite upstream velocity U_∞ is used and the length scale is chosen as $L = \sqrt{Rv/U_\infty}$, where R is the local radius of wall curvature and v is the kinematic viscosity. The local Reynolds number $Re = U_\infty L/v$ is then equal to the local dimensionless radius of wall curvature $r = R/L$. The length

Received March 19, 1992; revision received Feb. 21, 1993; accepted for publication Feb. 21, 1993.

*Graduate Research Assistant, Department of Mechanical and Aerospace Engineering; currently, Research Scientist, High Technology Corp., 28 Research Drive, P.O. Box 7262, Hampton, VA 23666.

†Professor, Department of Mechanical and Aerospace Engineering. Associate Fellow AIAA.

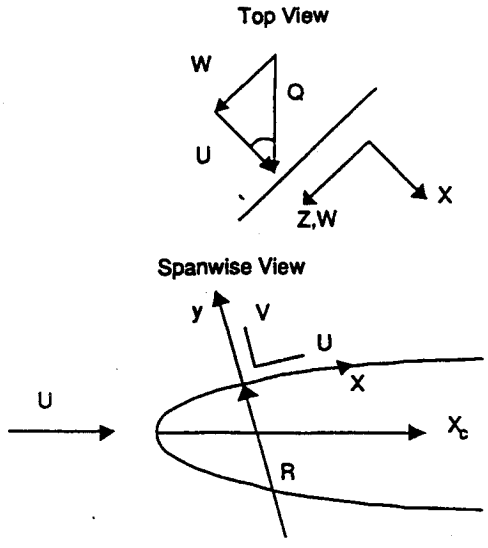

Fig. 1 Coordinate system for swept wing.

scale so defined allows the identification of the higher order terms in the disturbance equations given later. This length scale is further justified for the configuration under consideration in Sec. V.A., where comparisons with the usual reference boundary-layer thickness $\delta_r = x/\sqrt{Re_x}$ are given.

Substituting Eq. (1) into the N-S equations, subtracting the basic-state information, and linearizing with respect to the small perturbations gives a set of disturbance equations. In body-intrinsic curvilinear coordinates, they are

$$\frac{\partial u'}{\partial t} + \frac{r}{r+y}\bar{U}\frac{\partial u'}{\partial x} + \sigma\frac{r}{r+y}u'\boxed{\frac{\partial \bar{U}}{\partial x}} + \bar{V}\frac{\partial u'}{\partial y} + v'\frac{\partial \bar{U}'}{\partial y} + \frac{\bar{V}}{r+y}u' + \frac{\bar{U}}{r+y}v' + \bar{W}\frac{\partial u'}{\partial z} = -\frac{r}{r+y}\frac{\partial p'}{\partial x} + \frac{1}{Re}\left\{\left(\frac{r}{r+y}\right)^2\frac{\partial^2 u'}{\partial x^2} - \left[\frac{ry}{r+y}\frac{\partial}{\partial x}\left(\frac{1}{r+y}\right)\right]\frac{\partial u'}{\partial x} + \frac{\partial^2 u'}{\partial y^2} + \frac{1}{r+y}\frac{\partial u'}{\partial y} + \frac{2r}{(r+y)^2}\frac{\partial v'}{\partial x} + \left[\frac{r}{r+y}\frac{\partial}{\partial x}\left(\frac{1}{r+y}\right)\right]v' - \frac{u'}{(r+y)^2} + \frac{\partial^2 u'}{\partial z^2}\right\} \quad (2)$$

$$\frac{\partial v'}{\partial t} + \frac{r}{r+y}\bar{U}\frac{\partial v'}{\partial x} + \sigma\frac{r}{r+y}u'\boxed{\frac{\partial \bar{V}}{\partial x}} + \bar{V}\frac{\partial v'}{\partial y} + v'\frac{\partial \bar{V}}{\partial y} - \frac{2\bar{U}}{r+y}u' + \bar{W}\frac{\partial v'}{\partial z} = -\frac{\partial p'}{\partial y} + \frac{1}{Re}\left\{\left(\frac{r}{r+y}\right)^2\frac{\partial^2 v'}{\partial x^2} - \left[\frac{ry}{r+y}\frac{\partial}{\partial x}\left(\frac{1}{r+y}\right)\right]\frac{\partial v'}{\partial x} + \frac{\partial^2 v'}{\partial y^2} + \frac{1}{r+y}\frac{\partial v'}{\partial y} - \frac{2r}{(r+y)^2}\frac{\partial u'}{\partial x} - \left[\frac{r}{r+y}\frac{\partial}{\partial x}\left(\frac{1}{r+y}\right)\right]u' - \frac{v'}{(r+y)^2} + \frac{\partial^2 v'}{\partial z^2}\right\} m \quad (3)$$

$$\frac{\partial w'}{\partial t} + \frac{r}{r+y}\bar{U}\frac{\partial w'}{\partial x} + \sigma\frac{r}{r+y}u'\boxed{\frac{\partial \bar{W}}{\partial x}} + \bar{V}\frac{\partial w'}{\partial y} + v'\frac{\partial \bar{W}}{\partial y} + \bar{W}\frac{\partial w'}{\partial z} = -\frac{\partial p'}{\partial z} + \frac{1}{Re}\left\{\left(\frac{r}{r+y}\right)^2\frac{\partial^2 w'}{\partial x^2} - \left[\frac{ry}{r+y}\frac{\partial}{\partial x}\left(\frac{1}{r+y}\right)\right]\frac{\partial w'}{\partial x} + \frac{\partial^2 w'}{\partial y^2} + \frac{1}{r+y}\frac{\partial w'}{\partial y} + \frac{\partial^2 w'}{\partial z^2}\right\} \quad (4)$$

$$\frac{r}{r+y}\frac{\partial u'}{\partial x} + \frac{\partial v'}{\partial y} + \frac{v'}{r+y} + \frac{\partial w'}{\partial z} = 0 \quad (5)$$

The boundary conditions are that u', v', and w' vanish at $y = 0, \infty$. Note that a parameter σ has been introduced, where $\sigma = 1$ or 0 to include or exclude streamline-curvature terms. When $\sigma = 1$, this is the set of equations designated as linear N-S (LNS) in Secs. IV and V that is also solved to provide comparisons with the linear stability theory described later. The designation without nonparallel terms (WONP) in Sec. V.B. refers to the solution of these equations with $\sigma = 0$.

For large Re, the system of Eqs. (2–5) can be further simplified by neglecting terms of order Re^{-2} and smaller. The neglect of these terms has very little effect on any of the eigenvalue calculations discussed later. This was verified by comparison with calculations in which these terms are retained.

Attention is restricted to regions where wall curvature $(1/r)$ behaves as a slowly varying function. Thus, $r(x)$ in Eqs. (2–5) is replaced by its local value.

In the usual, linear, parallel stability theory, the basic state is assumed to change slowly in the streamwise coordinate direction. Therefore, the gradients of the basic-state properties in this direction are usually considered as higher order terms and are routinely neglected from the formulation. That reduces the system of equations from partial differential equations (PDE) to ordinary differential equations (ODE). However, most of the streamline-curvature effect is missing when the terms indicated in boxes in Eqs. (2–4) are dropped. In this study, in contrast to previous efforts, both the basic state and the gradients of the basic state are assumed to be slowly varying functions in the x direction. The basic-state velocities are approximated by their local values, and, to recover part of the streamline-curvature effect, the boxed terms in Eqs. (2–4) are retained in this formulation and approximated by their local finite difference values.

Following the assumptions made earlier, Eqs. (2–5) give a set of equations that is separable in the variables x, z, and t. As a result, the disturbance quantities can be expressed in the form

$$(u', v', w', p') = [\hat{u}(y), \hat{v}(y), \hat{w}(y), \hat{p}(y)]\exp^{i(\alpha_1 x + \beta z - \Omega t)} \quad (6)$$

Under the normal-mode assumption, Eqs. (2–5) become [neglecting the terms of $\mathcal{O}(Re^{-2})$]

$$\left[i(\alpha\bar{U} + \beta\bar{W} - \Omega) + \frac{1}{Re}(\alpha^2 + \beta^2) + \sigma\frac{r}{r+y}\boxed{\frac{\partial \bar{U}}{\partial x}} + \frac{\bar{V}}{r+y}\right]\hat{u} + \bar{V}\mathrm{D}\hat{u} - \left(\frac{1}{Re}\right)\mathrm{D}^2\hat{u} + \left(\mathrm{D}\bar{U} + \frac{\bar{U}}{r+y}\right)\hat{v} + i\alpha\hat{p} = 0 \quad (7)$$

$$\left[i(\alpha\bar{U} + \beta\bar{W} - \Omega) + \frac{1}{Re}(\alpha^2 + \beta^2) + \mathrm{D}\bar{V}\right]\hat{v} + \bar{V}\mathrm{D}\hat{v} - \left(\frac{1}{Re}\right)\mathrm{D}^2\hat{v} + \left(\sigma\frac{r}{r+y}\boxed{\frac{\partial \bar{V}}{\partial x}} - \frac{2\bar{U}}{r+y}\right)\hat{u} + \mathrm{D}\hat{p} = 0 \quad (8)$$

$$\left[i(\alpha\bar{U} + \beta\bar{W} - \Omega) + \frac{1}{Re}(\alpha^2 + \beta^2)\right]\hat{w} + \bar{V}\mathrm{D}\hat{w} - \left(\frac{1}{Re}\right)\mathrm{D}^2\hat{w} + \left(\sigma\frac{r}{r+y}\boxed{\frac{\partial \bar{W}}{\partial x}}\right)\hat{u} + (\mathrm{D}\bar{W})\hat{v} + i\beta\hat{p} = 0 \quad (9)$$

$$i\alpha\hat{u} + \mathrm{D}\hat{v} + \left(\frac{1}{r+y}\right)\hat{v} + i\beta\hat{w} = 0 \quad (10)$$

where D = d/dy and $\alpha = \alpha_1 r/(r + y)$. Note that the parameter σ has been retained, where $\sigma = 1$ or 0 to include or exclude the streamline-curvature terms. For $\sigma = 1$ and 0, the solution of this set of equations is designated bdy11 and bdy01, respectively, in Sec. V.B.

The boundary conditions for the previous sixth-order system, Eqs. (7–10), are

$$\hat{u} = \hat{v} = \hat{w} = 0, \qquad y = 0, \infty \tag{11}$$

Also note that if the wall curvature, streamline curvature, and the normal velocity component of the basic state are neglected, the previous system of equations reduces to the fourth-order Orr-Sommerfeld (O-S) equation by Squire's transformation:

$$\Phi'''' - 2\alpha_0^2\Phi'' + \alpha_0^4\Phi = iR\left[(\alpha_0 U_0 - \Omega)(\Phi'' - \alpha_0^2\Phi) - \alpha_0 U_0''\Phi\right] \tag{12}$$

and the boundary conditions become

$$\Phi = \Phi' = 0, \qquad y = 0, \infty \tag{13}$$

The solution of this system is designated O-S in Sec. V.B.

III. Numerical Method

To study the wall-curvature and streamline-curvature effects, numerical results will be presented for both the sixth-order system, Eqs. (7–11), and the fourth-order system, Eqs. (12) and (13).

The Chebyshev collocation method is used to solve the governing linear-stability equations and the associated boundary conditions on a set of Gauss-Labato points, $\eta_j = \cos \pi j/M$, where M is the total number of collocation points. The normal coordinate y ($0 \le y \le Ye$) is mapped into the finite interval $-1 \le \eta \le 1$ by a stretching mapping function

$$\eta = \frac{A}{y+h} + B + Cy \tag{14}$$

where

$$A = \frac{2h(Ye+h)(Ye-2h)}{Ye(Ye-h)}, \qquad B = \frac{h-A}{h}, \qquad C = \frac{A-2h}{2h^2}$$

In the following calculations, the far-field homogeneous velocity perturbation boundary conditions are imposed at $Ye = 20\delta$, and the stretching parameter $h = 0.1Ye$ is used for an appropriate distribution of grid points in the physical domain. In most of the calculations reported later, M is chosen as 41 (see Table 1). The resulting eigenvalue problems are solved by a local iteration scheme.[11]

IV. Linear Navier-Stokes Calculations

To validate the theory described in Sec. II, the linear disturbance PDEs, Eqs. (2–5), are solved by direct numerical integration. This set of equations has accuracy up to the nonlinear terms for the disturbances and is freed from any assumption for the basic state (except conical flow), the wall curvature, or the behavior of the disturbance-shape function and wave number. Here the effects of the streamline curvature as well as the wall curvature are treated exactly up to the order of the numerical truncation errors ($\sigma = 1$, designated LNS). To be able to identify the effect of streamline curvature, the equations are solved again but with all of the nonparallel terms neglected ($\sigma = 0$, designated WONP). Since all of the spatially variable coefficients in Eqs. (2–5) are functions of x and y only, it is appropriate to consider linear disturbances of the form

$$q'(x, y, z, t) = \hat{q}(x, y, t)\exp(i\beta z) + \text{c.c.} \tag{15}$$

where $q' = (u', v', w', p')$, and β is real, and c.c. stands for complex conjugate. Substituting Eq. (15) into Eqs. (2–5) leads to a system of equations for the wave number β in a two-dimensional (x, y) domain. Although the problem of stationary crossflow vortices renders a steady-state solution, the time-derivative terms are retained in the equations because a transient approach will be used to solve the problem.

The boundary conditions for the linear N-S calculations are as follows. At the far field, $y = y_\infty$, all disturbances are assumed to be zero, and therefore, for all disturbance variables,

$$q'(x, y_\infty, z, t) = 0$$

Along the stagnation (or symmetric) line, u' is set to be zero, whereas v' and w' are assumed to be symmetric with respect to the stagnation line. On the wall surface, no-slip conditions are used,

$$u'(x, 0, z, t) = w'(x, 0, z, t) = v'(x, 0, z, t) = 0$$

However, on a specified portion of the surface ($x_0 < x < x_1$), the v' component is prescribed as a function of x, z, and t,

$$v'(x, 0, z, t) = \varepsilon A_v(x) T_v(t)\cos(\beta z) \tag{16}$$

where $t > 0$. Typical forms of $A_v(x)$ and $T_v(t)$ are given in Fig. 2, and β is the chosen wave number to be examined. This allows the introduction of localized steady blowing and suction at the surface to stimulate an instability. At the downstream boundary, $x = x_{max}$, the second derivatives with respect to x are set to zero, $\partial^2 q'/\partial x^2 = 0$. For the configurations considered in this work, this boundary condition works well as long as x_{max} is reasonably large. To discretize the resulting system of equations, finite difference approximations of second-order accuracy are used in the x and y directions. The time derivatives are approximated with a Crank-Nicolson method. Thus, the method is implicit and of second-order accuracy. The time step is chosen as $\Delta t = 0.002$ to ensure numerical stability. The simulation uses up to 8,000 time steps, and consumes about 60 CPU h on a single processor of a CRAY X-MP/116se.

Table 1 Effect of number of collocation points M on complex wave number $\alpha_1 = \alpha_r + i\alpha_i$

M	α_r	α_i
13	0.742342	$+0.16016 \times 10^{-2}$
21	0.741874	-0.50940×10^{-2}
29	0.742030	-0.48332×10^{-2}
36	0.742059	-0.48313×10^{-2}
41	0.742059	-0.48309×10^{-2}
61	0.742059	-0.48310×10^{-2}

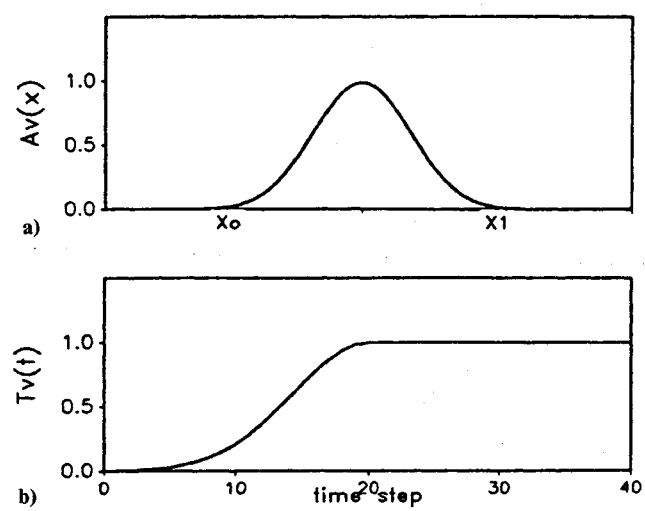

Fig. 2 a) Amplitude-distribution function, $A_v(x)$ and b) amplitude-rising function, $T_v(t)$, of normal-velocity component for quasisteady blowing-suction strip.

V. Results

A. Basic State

To demonstrate the new theory of Sec. II, the incompressible, laminar boundary-layer flow over an infinite-span swept wing is considered. The symmetric wing at 0-deg incidence has a half-thickness of 6 cm; its surface consists of a 5:1 elliptic leading-edge portion followed by a flat plate; however, in the juncture region the elliptic surface is gradually replaced by a smooth polynomial surface to remove the discontinuity of the wall curvature. The freestream speed is 35 m/s, and a sweep angle of 70 deg is chosen to maximize the instability (as discussed later) and to provide substantial streamline curvature in the leading-edge region.

For this configuration, the length scale chosen in Sec. II $L = \sqrt{Rv/U_\infty}$ where R is the local radius of wall curvature, is compared with the length scale usually chosen for stability work, $\delta_r = x/\sqrt{Re_x}$ in Table 2. From this it is seen that L is of the same order as δ_r in the leading-edge region, where surface curvature and streamline curvature are important and the crossflow instability is expected to dominate, and is therefore a reasonable length scale to use for the linear stability analyses of this work. Moreover, as stated before, the use of L will make the relative sizes of the terms in the equations more apparent in this study.

The N-S equations and associated boundary conditions in primitive-variable form are discretized by a second-order finite difference method over a staggered grid. The mesh size is 320×128 in the x and y directions, respectively. Under this setup, there is no need for any artificial pressure boundary condition. The pressure Poisson equation is solved by a highly efficient five-level multigrid method and the momentum equations are solved by a line successive over-relaxation (LSOR) scheme. Further numerical details are available in Lin and Reed.[12]

The resulting wall pressure distribution is shown in Fig. 3a. More than 50% of the nose region is under a favorable pressure gradient. The maximum (in magnitude) crossflow speed, w_{max} (perpendicular to the local inviscid direction), ranges between 2 and 5% of the local inviscid speed U_e in the leading-edge region as seen in Fig. 3b. Figure 4a shows the angle between the local inviscid direction and the x axis. This plot indicates that the inviscid streamlines bend severely in the nose region and then become rather straight aft. Figure 4b shows the gradient of the wall curvature in the x direction in the leading-edge region. This plot indicates that the previous approximation of slowly varying wall curvature is valid over most of the curved surface except at the very front. However, the crossflow Reynolds numbers are low in this region and the stationary crossflow instability is not expected to be important.

Two dimensionless parameters commonly used both in experiment and theory to correlate crossflow-vortex appearance with freestream and boundary-layer conditions are the local crossflow Reynolds number, $R_{cf} = w_{max}y_{10}/v$, and local shape factor, $H_{cf} = y_{max}/y_{10}$, based on the maximum (in magnitude) crossflow velocity w_{max}, its normal-to-the-wall location y_{max}, and the location y_{10} above y_{max} where the crossflow velocity is 10% of the maximum. Distributions of these plotted vs chordwise distance from the leading edge are shown in Figs. 5a and 5b, respectively. Stationary vortices normally seem to appear when crossflow Reynolds numbers

Table 2 Comparison of L with δ_r

X, cm	δ_r, cm	L, cm	L/δ_r
0.23	0.005	0.016	3.2
1.71	0.015	0.032	2.1
5.51	0.026	0.061	2.3
10.11	0.036	0.087	2.4
14.77	0.043	0.096	2.2
19.47	0.049	0.106	2.2
21.83	0.052	0.121	2.3
24.19	0.055	0.153	2.8
26.55	0.058	0.235	4.1
28.43	0.060	0.487	8.1

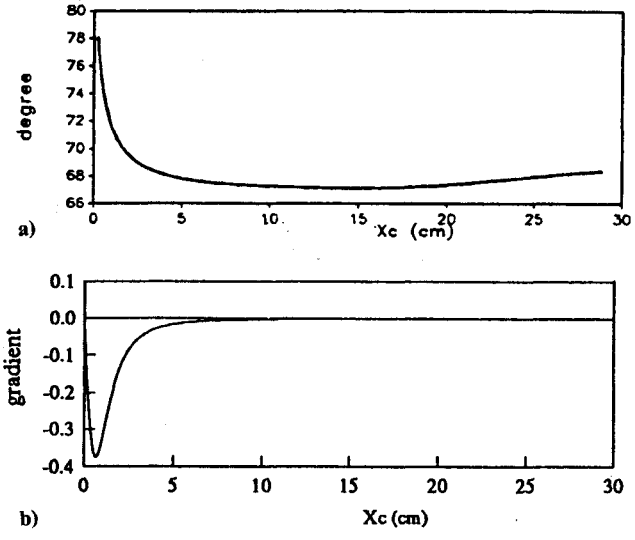

Fig. 4 Variation of a) local inviscid streamline direction and b) wall-curvature gradient, d(1/r)/dx.

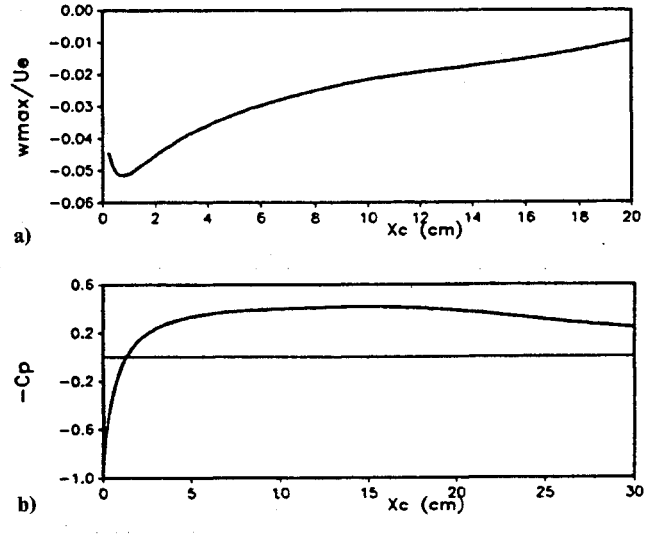

Fig. 3 a) Pressure-coefficient distribution along the surface and b) variation of the local maximum (in magnitude) of crossflow velocity.

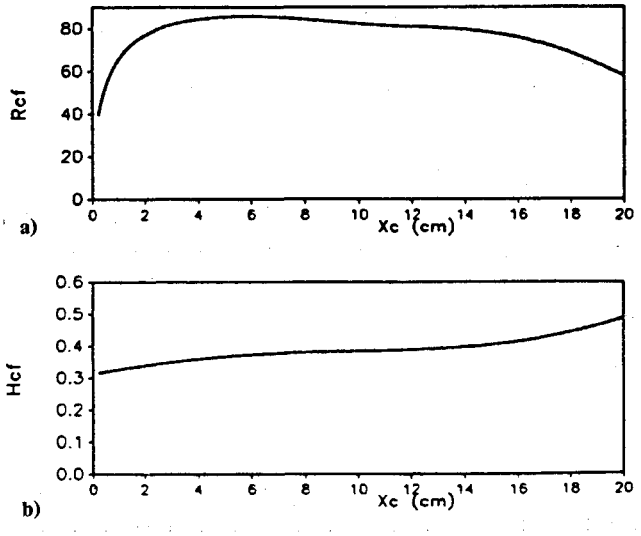

Fig. 5 Variation of a) crossflow Reynolds number and b) crossflow shape factor.

are on the order of 100 and shape factors are on the order of 0.3 (Ref. 13).

B. Linear Disturbance Calculations

This section contains a discussion and comparison of the linear disturbance calculations using the different formulations mentioned earlier: 1) O-S: Orr-Sommerfeld—no curvature, 2) bdy01: new linear stability theory—body curvature only ($\sigma = 0$), 3) bdy11: new linear stability theory—body and streamline curvature ($\sigma = 1$), 4) LNS: linear N-S with nonparallel terms—body and streamline curvature ($\sigma = 1$), and 5) WONP: linear N-S without nonparallel terms—body curvature only ($\sigma = 0$). In all cases, the basic state is provided by the full N-S simulation mentioned in Sec.V.A.

Since the instability is spatial in nature, all of the analyses are based on the spatial theory. The spatial growth rates reported here are obtained by solving nonlinear eigenvalue problems rather than transforming temporal growth rates using the group velocity. Considering that the wing has an infinite span, the stationary crossflow vortices are assumed to have no growth in the spanwise direction.[14] This assumption is represented by setting $\beta_i = 0$ in Eq. (6).

First, the most unstable wave angles are examined for formulations 1–3, linear stability theory with different combinations of streamline and body curvature. Here, wave angle is designated as the angle between the x axis and the wave number vector, $\boldsymbol{n} = (\alpha_r, \beta_r)$. Results show that the curvature only has a minor effect on the wave angles. The direction of the most unstable stationary wave predicted by the present theory is only about 1 deg different from that predicted by the Orr-Sommerfeld equation. This result is consistent over the domain of interest.

In Figs. 6a and 6b, spatial growth rates are plotted vs wavelength for formulations 1–3, where wavelength is measured in the direction normal to the axis of the vortex. The inclusion of the wall curvature decreases the most unstable spatial growth rate, especially in the upstream region where the radius of wall curvature is smaller. On the other hand, the inclusion of streamline curvature increases the growth rates. Also note that this destabilizing effect of the streamline curvature over the surface curvature is increasingly stronger in the downstream direction. To account for this phenomenon, the comparison between the magnitude of nonparallel terms and $1/Re$ is provided in Table 3. Results show that the contribution of the nonparallel terms (the source of the streamline-curvature effect) increases in the downstream direction. Nonparallel terms are of the order of $1/Re$ over the leading-edge region, i.e., $x < 20$ cm, and eventually grow out of the order of $1/Re$ in the region where the boundary-layer thickness increases rapidly and the crossflow changes sign due to the reverse of the pressure gradient.

To illustrate the effect of curvature on N factor, calculations are performed by using the fixed wavelength (λ_z in spanwise direction) method.[15,16] Thus, the N factor is defined as

$$N = \ell_n (A/A_0) = -\int_{x_I}^{x} \alpha_i \, dl$$

where dl is the arclength along the curved surface and A and A_0 are the disturbance amplitudes at x and x_I (branch I), respectively.

The comparisons of the N factors for formulations 1–3 are given in Fig. 7, where fixed-wavelength results for $\lambda_z = 3$ cm are shown. Note, $\lambda_z = 3$ cm corresponds to the most amplified mode which has wavelength about 1.2 cm measured normal to the axis of the vortex. The N factors predicted by the present theory are smaller than those predicted by the Orr-Sommerfeld equation. On the other hand, the inclusion of the streamline-curvature effect only causes a relatively mild increase in the N factors over the results including just the body curvature. This is consistent with the evidence shown in Table 3.

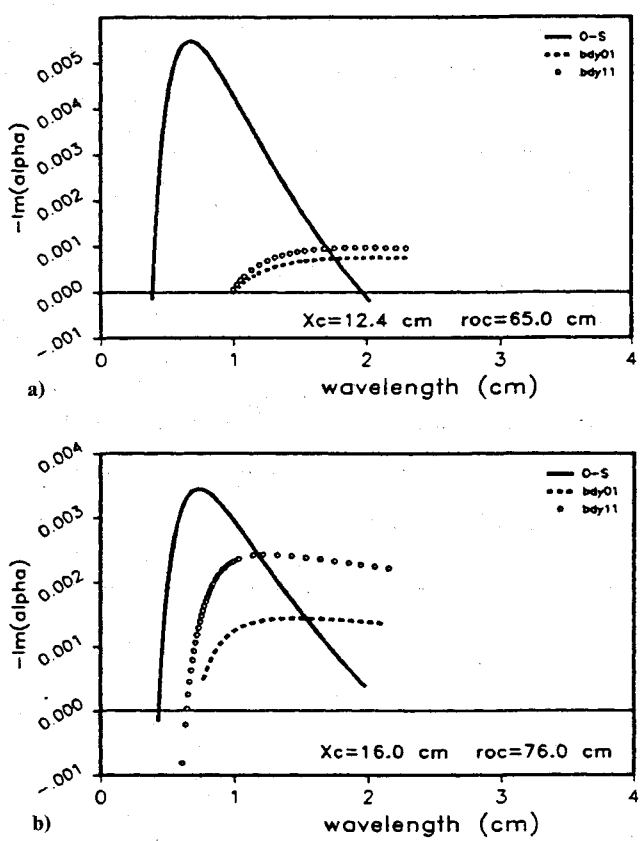

Fig. 6 Distribution of spatial growth rate with wavelength at a) Xc = 12.4 cm, radius of curvature (roc) = 65 cm and b) Xc = 16 cm, roc = 76 cm. O-S (—), without curvature effects; bdy01 (- - -), with wall-curvature effects; bdy11 (o), with both streamline- and wall-curvature effects.

Table 3 Comparison of nonparallel terms with $1/Re$

x, cm	$a = (1/Re)$	b[a]	$c = b/a$
0.23	0.77E-2	0.79E-2	1.0
3.37	0.27E-2	0.87E-2	3.2
7.80	0.17E-2	0.73E-2	4.3
12.44	0.13E-2	0.57E-2	4.3
17.12	0.13E-2	0.65E-2	5.2
19.47	0.12E-2	0.82E-2	7.0
21.83	0.10E-2	0.11E-1	10.4
24.19	0.82E-3	0.14E-1	16.6
26.55	0.53E-3	0.16E-1	29.5
28.43	0.26E-3	0.18E-1	69.4

[a]Where $b = \max\left(\partial\bar{U}/\partial x, \partial\bar{V}/\partial x, \partial\bar{W}/\partial x\right)$.

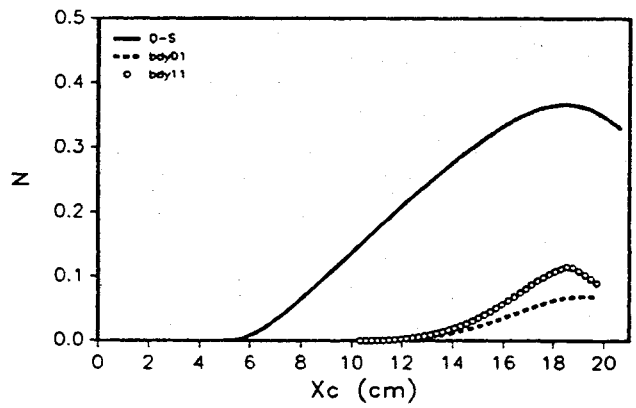

Fig. 7 N factor calculations for $\lambda_z = 3$ cm with various linear stability theories O-S (—), without curvature effects; bdy01 (- - -), with wall-curvature effects; bdy11 (o), with both streamline- and wall-curvature effects.

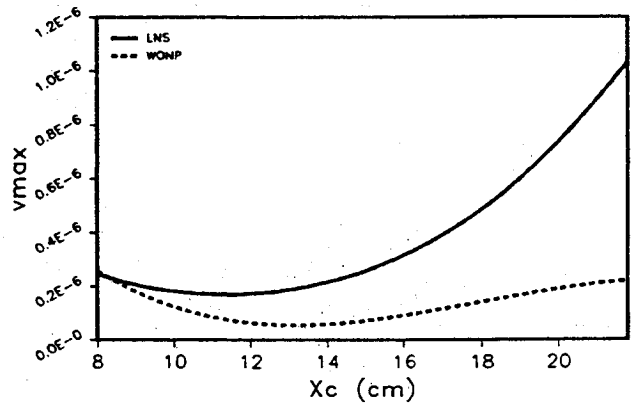

Fig. 8 Comparison of the local maximum of the disturbance in the normal direction ν_{max} of the linear N-S calculation: LNS (—), solution of the full linear N-S equations; WONP (- - -), solution of the linear N-S equations without the nonparallel terms.

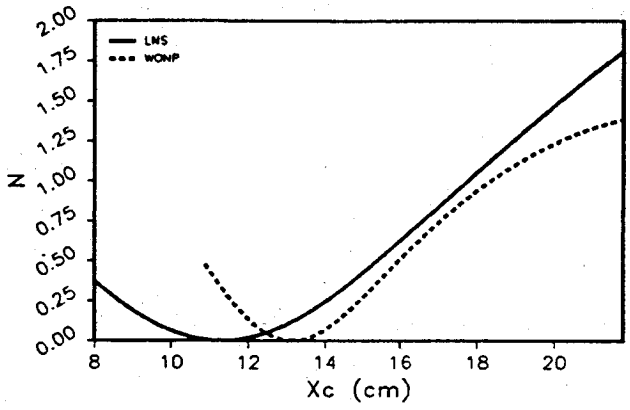

Fig. 9 Amplification curves of the linear N-S calculations based on ν_{max}: LNS (—), solution of the full linear N-S equations; WONP (- - -), solution of the linear N-S equations without the nonparallel terms.

Moreover, it must be emphasized that Table 3 demonstrates that the relative effects (to each other) of streamline curvature and body curvature vary with streamwise position and must be evaluated for each configuration under consideration. For this configuration, the body curvature is stabilizing and the subsequent inclusion of streamline curvature on top of this has less of a destabilizing effect toward the front than farther downstream.

To validate the results, the linear N-S equations are solved as an initial boundary-value problem by direct numerical integration. To apply these results to those mentioned earlier, λ_z is chosen to be 3 cm. To minimize the contribution of nonlinear terms, ε is set as $1.0E$-5 in Eq. (16). Moreover, the quasisteady blowing-suction slot is located at $5.5 \le x \le 6.9$ cm, before the branch I predicted by the present theory. A steady solution over the domain of interest was obtained, and results are summarized in Figs. 8 and 9.

Figure 8 shows that the disturbance amplitudes given by the linear N-S equations with nonparallel terms neglected are everywhere smaller than those predicted by the full linear N-S equations. This confirms that the effect of nonparallel terms (streamline curvature) is destabilizing. However, any attempt to compare the N factors from the theory and the linear N-S calculations is very difficult, because the linear N-S equations contain the nonparallel effect exactly. Therefore, the N factors can depend a great deal on definition. This issue has been addressed by Fasel and Konzelmann.[17] Nevertheless, in Fig. 9, an N factor is determined for the computations based on the local maximum of the disturbance in the normal direction. In comparison with the computations, the present theory with both body and streamline curvature included predicts a better branch I location. However, all three theories predict an earlier branch II at the location where the pressure gradient first changes sign, whereas the computations show unstable behavior farther downstream. This indicates that a more consistent approximation is needed when the effect of nonparallel terms becomes non-negligible (Table 3).

VI. Concluding Remarks

This paper addresses the wall-curvature and streamline-curvature effects on the stationary crossflow instability of a swept-wing boundary layer. The disturbance equations are written on a fixed body-intrinsic coordinate system; thus the wall curvature is consistently formulated. Results indicate that curvature has only a minor effect on wave angle. By representing the nonparallel terms with a finite-difference approximation and comparing with the solutions of the O-S equation, wall curvature is found to be stabilizing and streamline curvature is found to be destabilizing for the stationary crossflow instability. Results are further verified by more expensive linear N-S calculations.

The current method breaks down when the contribution from nonparallel terms becomes non-negligible. Then a more consistent approximation is required. But the linear N-S calculations are too expensive to be useful for engineering application. The recent parabolized stability equations method[18] can be a substitute; however, at this time, it is not clear from the present work how successful the disturbance-shape function can be considered as a slowly varying function in swept-wing flow.

The strength of linear theories is in their use for design by comparing N factors from one configuration to another. A configuration with a smaller N factor (using the same theory) is likely to remain laminar longer. It has been demonstrated here that the new theory at least qualitatively contains the appropriate relationships between body and streamline curvature for three-dimensional boundary layers and in this sense will aid in the evaluation of new airfoil shapes for swept wings.

Acknowledgments

This work was supported by NASA Langley Research Center under a graduate fellowship in aeronautics. The second author is grateful to the Institute of Fluid Science, Tohoku University, Sendai, Japan, for her support during her sabbatical there.

References

[1]Reed, H. L., and Saric, W. S., "Stability of Three-Dimensional Boundary Layers," *Annual Review of Fluid Mechanics*, Vol. 21, No. 1, 1989, pp. 235–284.

[2]Bippes, H., "Instability Features Appearing on Swept-Wing Configurations," *Laminar-Turbulent Transition*, edited by D. Arnal and R. Michel, Vol. III, Springer-Verlag, Berlin, 1990, pp. 419-430.

[3]Kohama, Y., Saric, W. S., and Hoos, J. A., "A High Frequency, Secondary Instability of Crossflow Vortices that Leads to Transition," *Proceedings of the Royal Aeronautical Society, Boundary Layer Transiton and Control*, The Royal Aeronautical Society, Cambridge, England, UK, April 1991, pp. 4.1–4.13.

[4]Radeztsky, R. H., Reibert, M. S., Saric, W. S., and Takagi, S., "Effect of Micron-Sized Roughness on Transition in Swept-Wing Flows," AIAA Paper 93-0076, Jan. 1993.

[5]Gregory, N., Stuart, J. T., and Walker, W. S., "On the Stability of Three-Dimensional Boundary Layers with Application to the Flow due to a Rotating Disk," *Philosophical Transactions of the Royal Society of London*, Series A, Vol. 248, 1955, pp. 155–199.

[6]Kobayashi, R., Kohama, Y., and Takamadate, C., "Spiral Vortices in Boundary Layer Transition Regime on a Rotating Disk," *Acta Mechanica*, Vol. 35, 1980, pp. 71–82.

[7]Malik, M. R., Wilkinson, S. P., and Orszag, S. A., "Instability and Transition in Rotating Disk Flow," *AIAA Journal*, Vol. 19, No. 9, 1981, pp. 1131–1138.

[8]Mack, L. M., "The Wave Pattern Produced by Point Source on a Rotating Disk," AIAA Paper 85-0490, Jan. 1985.

[9]Spalart, P. R., "On the Cross-Flow Instability Near a Rotating Disk," *Proceedings of the Royal Aeronautical Society, Boundary Layer Transiton and Control*, The Royal Aeronautical Society, Cambridge, England, UK, April 1991, pp. 22.1–22.13.

[10]Malik, M. R., and Poll, D. I. A., "Effect of Curvature on Three-Dimensional Boundary Layer Stability," AIAA Paper 84-1672, June 1984.

[11]Malik, M. R., Chuang, S., and Hussaini, M. Y., "Accurate Numerical Solution of Compressible, Linear Stability Equations," *Journal of Applied Mathematics and Physics (ZAMP)*, Vol. 33, March 1982, pp. 189-201.

[12]Lin, R.-S., and Reed, H. L., "Direct Numerical Simulation of Stationary Crossflow Instability in a Swept-Wing Boundary Layer" (in preparation).

[13]Pfenninger, W., "USAF and Navy-Sponsored Northrop LFC Research between 1949 and 1967," AGARD/VKI, Special Course for Drag Reduction, Rept. No. 654, von Kármán Inst., Rhode-St-Genese, Belgium, March 28–April 1, 1977.

[14]Mack, L. M., "On the Stabilization of Three-Dimensional Boundary Layers by Suction and Cooling," *Laminar-Turbulent Transition*, edited by R. Eppler and H. Fasel, Springer-Verlag, Berlin, 1980, pp. 223–238.

[15]Mack, L. M., "On the Stability of the Boundary Layer on a Transonic Swept Wing," AIAA Paper 79-0264, Jan. 1979.

[16]Mack, L. M., "Stability of Three-Dimensional Boundary Layers on Swept Wings at Transonic Speeds," *IUTAM Symposium Transsonicum III* (Gottingen), edited by J. Zierep and H. Oertel, Springer-Verlag, Berlin, May 1988.

[17]Fasel, H., and Konzelmann, U., "Non-Parallel Stability of a Flat-Plate Boundary Layer Using the Complete Navier-Stokes Equations," *Journal of Fluid Mechanics*, Vol. 221, Dec. 1990, pp. 311–347.

[18]Herbert, T., "Boundary-Layer Transition Analysis and Prediction Revisited," AIAA Paper 91-0737, Jan. 1991.